6th International Conference on Advances in Experimental Structural Engineering
11th International Workshop on Advanced Smart Materials and Smart Structures Technology
August 1-2, 2015, University of Illinois, Urbana-Champaign, United States

Thermo-, Chemo-, and Mechano-Optical Characterization of Multi-Modal Tensile Strain and pH Sensing Thin Films

D. Ryu[1]*, M. Romero[2], and R. Stoer[2]

1 Assistant Professor, Dept. of Mechanical Engineering, New Mexico Tech, Socorro, NM, United States.
**E-mail: dryu@nmt.edu*
2 Undergraduate Student, Dept. of Mechanical Engineering, New Mexico Tech, Socorro, NM, United States.

ABSTRACT
In this study, multiphysics properties (*i.e.*, thermo-, mechano-, and chemo-optical properties) of the multi-modal sensing thin films were characterized using ultraviolet-visible (UV-Vis) spectrophotometer and X-ray diffractometer (XRD). First, multi-modal tensile strain and pH sensing thin films were fabricated using poly(3-hexylthiophene) (P3HT) and polyaniline (PANI) conjugated polymers, respectively. Second, crystalline structures of the P3HT molecules in the P3HT-based thin films were characterized using XRD. Second, light absorptivity of P3HT-based thin films was acquired at various annealing temperature to study its thermo-optical properties. Last, chemo- and mechano-optical properties of PANI-based thin films were characterized using UV-Vis spectrophotometer by acquiring light transmittance at various pH levels and tensile strains.

KEYWORDS: *P3HT, PANI, UV-Vis, multi-modal sensing, multiphysics characterization, XRD*

1. INTRODUCTION

Infrastructures are subjected to various types of external stimuli (*e.g.*, excessive deformations, cyclic loadings, and chemical intrusions, among many others). These often trigger deteriorations of structural materials and initiate damage in the structural systems. If the damage occurrence is not detected in timely manner, the infrastructures can collapse. For preventing the catastrophic failures of the infrastructures, structural health monitoring (SHM) has been suggested, and advanced sensing technologies allowed reliable monitoring and damage detection of the infrastructures in SHM [1-4]. Nevertheless, the state-of-the-art sensing technologies suffer from limitations. For example, the current sensing technologies require external electrical energy supply, and each sensor can detect only one type of physical phenomena (*e.g.*, mechanical, thermo, and chemical phenomenon, among many others).

Deterioration and failure of structural systems are not attributed to only one type of physical phenomena. For example, steel structures' design strength can be degraded due to excessive loading as well as corrosion. Yet, current methodologies for the multiphysics damage detection are instrumentation of a variety of sensors so that each sensor can measure a certain physical response or estimation of the extent of degradation in structural component based on dimensional changes [5-8]. But, as the number of sensors employed increases, cost for installation of sensors, computation, and energy consumption increases. Monitoring based on dimensional changes is still limited because it can hardly distinguish which was attributed to the deteriorations. Information of dimensional changes could be deficient to be used for reliable prognosis. So, required is a new sensing technology capable of selectively sensing various physical phenomena (*i.e.*, mechanical and chemical stimuli).

Multi-modal and photoactive structural coatings were suggested by Ryu and Loh [9] to measure tensile strain and pH for detecting cracks and corrosion, respectively. The structural coatings were fabricated using conjugated poly(3-hexylthiophene) (P3HT) and polyaniline (PANI) polymers. It was shown that the photoactive structural coatings could selectively sense tensile strain and pH by measuring changes of the electrical current (*i.e.*, photocurrent) generated under blue- and infrared-light, respectively. The photocurrent-based multi-modal sensing was enabled due to intrinsic optical properties of P3HT and PANI, which were affected by tensile strain and pH. It is hypothesized that the multiphysics external stimuli (*i.e.*, tensile strain and pH) affect crystalline nanostructures and oxidation status of the conjugated P3HT and PANI polymers.

The principal goal of this study is to understand multiphysics properties of two sensing thin films, which are P3HT- and PANI-based thin film and constitute photoactive multi-modal thin film sensors. To obtain the goal,

P3HT- and PANI-based thin films were characterized using ultraviolet-visible (UV-Vis) spectrophotometer and X-ray diffractometer (XRD) at various conditions (*i.e.*, annealing temperature, pH, and tensile strain). First, the P3HT-based and PANI-based sensing thin films were fabricated using spin-coating and layer-by-layer (LbL) thin film deposition technique, respectively. Second, thermo-optoelectronic properties of the P3HT-based tensile strain sensing thin films were characterized using UV-Vis and XRD. The P3HT-based thin films were annealed at various temperatures for different time duration, and light absorptivity was acquired using UV-Vis. The P3HT conjugated polymers' crystalline structures were studied using XRD. Third, chemo-optical properties of PANI-based thin films were studied by obtaining light transmittance of PANI-based thin film on which a full range of pH was simulated. Last, the PANI-based thin films were subjected to tensile strain loading/unloading, and light transmittance of PANI-based thin films were acquired at various tensile strains for studying mechano-optical properties.

2. EXPERIMENTAL DETAILS

2.1. Materials

P3HT (Regioregularity: 93 – 95%; M_w: 50 – 70 *kDa*) and [6,6]-phenyl-C61-butyric acid methyl ester (PCBM; purity>99.5%) were obtained from Solaris Chem Inc. PANI (emeraldine base; M_w: ~65 *kDa*), poly(sodium 4-styrenesulfonate) (PSS; M_w: ~1 *MDa*), N,N-dimethylformamide (DMF, purity>99.8%), and 1,2-dichlorobenzene (DCB) were acquired from Sigma-Aldrich. Polydimethylsiloxane (PDMS) was obtained from Dow-Corning. pH buffers, solvents, and supplies used were purchased from Fisher Scientific.

2.2. Solutions preparation

Three different types of solutions were prepared and used for fabricating thin films, which consisting of multi-modal tensile strain and pH thin film sensors [9]. First, prepared were three different sets of P3HT/PCBM-DCB solutions, which have various mixing ratio of P3HT and PCBM to yield three different concentrations: 1:0.5, 1:1, and 1:1.5 *w/v*%. P3HT and PCBM were weighed accordingly and dissolved in DCB and heated/stirred at 40 °C for 24 h. Then, the P3HT/PCBM-DCB solutions were filtered using syringeless filters. Each set of P3HT/PCBM-DCB solutions is named as #1, #2, and #3 PPD in the order of increasing PCBM concentration. Second, 0.1 *w/v*% PANI-DMF/deionized (DI) water solution was prepared. Emeraldine base PANI was weighed and dissolved in DMF to prepare 1 *w/v*% PANI-DMF solution, which was subjected to heating at 40°C for 48 h and stirring, followed by filtration to eliminate possible agglomeration of PANI. The PANI in DMF solution was diluted tenfold with DI water. The emeraldine base PANI in the diluted solution was protonated to emeraldine salt form after the pH of the PANI-DMF/DI was adjusted to be ~2.5 by adding drops of 10 *v*% hydrochloric acid. Last, 1 *w/v*% PSS-DI was prepared by subjecting PSS in DI water for 30 min without heating.

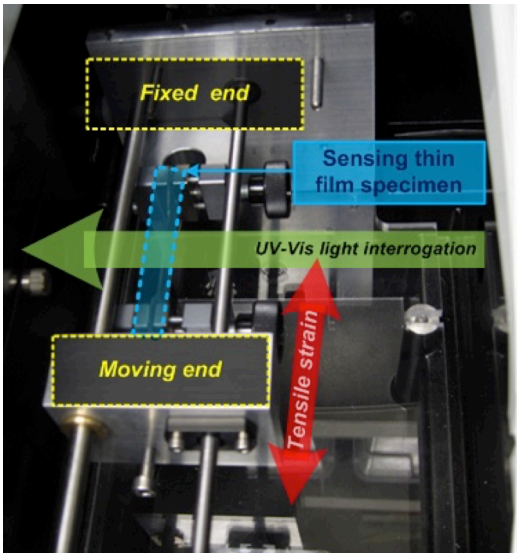

Figure 2.1 Custom-built load frame is integrated with UV-Vis spectrophotometer to measure mechano-optical properties of sensing thin film specimens.

2.3. Thin film specimens fabrication

P3HT- and PANI-based thin film specimens were prepared on glass slides (dimension: 25×75 mm^2) and PDMS substrates using the prepared solutions in Section 2.2. Glass slides were wet-cleaned using acetone and isopropyl alcohol in a bath sonicator and dry-cleaned using a UV-ozone cleaner. 1 mm thick PDMS substrates were prepared on silicone wafers (diameter: 10 mm) by following the procedure used by Ryu and Loh [9]. Argon plasma treatment was used for decreasing surface energy of PDMS substrate and facilitating P3HT-based thin film fabrication.

First, three different sets of P3HT-based thin film specimens were spin-coated on glass slides and PDMS substrates by spreading the #1, #2, and #3 PPD solutions at 500 rpm for 5 s and coating at 1,300 rpm for 60 s. The spin-coated P3HT-based thin film specimens were annealed at various temperate and for various time durations depending the purpose of each research task. P3HT-based thin films on PDMS substrates were cut into dog-bone shape with 39 mm gage length.

Second, layer-by-layer (LbL) thin film fabrication technique was employed for fabricating PANI-based thin films on glass slides and PDMS substrates. First, a substrate (*i.e.*, either glass slide or PDMS substrate) was immersed in PANI-DMF/DI solution for 3 min. Any excessive PANI emeraldine salt was rinsed off with DI water and air-dried. Next, the one layer of PANI thin film coated substrate was immersed in PSS solution for 3 min, followed by rinsing with DI water and air-drying. This completes one bilayer consisting of emeraldine salt PANI and PSS, and this procedure was repeated to complete the desired number of bilayers of PANI-based pH sensing thin films on glass slides and PDMS substrates. The PANI-based thin films on PDMS substrates were cut into dog-bone shape (gage length: 39 mm).

2.4. X-ray crystallographic analysis

The #2 P3HT-based thin film on PDMS specimen was analyzed using Scintag XDS2000. Again, the specimen was prepared on PDMS substrate using #2 PPD solution, which was annealed at 80°C for 60 min. The #2 P3HT-based thin film was placed on a glass slide without being stretched and mounted in the Scintag XDS 2000. The unstrained P3HT-based thin film was interrogated by X-ray with incident angle from 1° to 7.5°. The number of X-ray diffracted by the P3HT molecules in the thin film specimen was counted by a detector in the identical range of the incident X-ray. So, total scanning range (2θ) was 2° - 15°.

2.5. UV-Vis spectroscopic analysis

Evolution 220 UV-Vis spectrophotometer was used for obtaining light absorptivity of P3HT-based thin film specimen and light transmittance of PANI-based thin film specimen under various conditions (*i.e.*, various annealing temperature, pH, and tensile strain).

First, thermo-optical properties of the P3HT-based thin film specimens prepared on glass slides were characterized. Three different P3HT-based thin films on glass slides, which were prepared using #1, #2, and #3 PPD solutions, were annealed at 150°C for various annealing time duration. Light absorbance spectrums of the three different P3HT-based thin films were obtained without annealing and after 10 min and 300 min annealing. While keeping the annealing time consistent to be 10 min, annealing temperature was varied from 70°C to 240°C.

Second, chemo-optical properties of the PANI-based thin film specimens were studied by obtaining light transmittance of the PANI-based thin films at various pH levels. PANI-based thin films were treated with thirteen different pH buffers to simulate various pH levels. Light transmittance of a pristine PANI-based thin film specimen on a glass slide (*i.e.*, without pH buffer treatment) was first obtained in 300 – 1,100 nm wavelength range. Then, pH 1 buffer was dispensed over the PANI-based thin film and left for 10 s and dried using a heat gun. Light transmittance spectrum of the pH 1 buffer-treated PANI-based thin film was acquired. The PANI-based thin film was treated by pH 2, 3, 4, 5, 6, 7, 8, 9, 10, 11, 12, and 13, sequentially. Light transmittance spectrum was obtained after each pH treatment.

Last, using the test setup shown in Fig. 2.1, mechano-optical properties of PANI-based sensing thin film specimens on PDMS substrates were investigated. Load frame was built to fit in the measurement chamber of the UV-Vis spectrophotometer; the load frame can precisely strain specimens with a 625 nm resolution. The PANI-based thin film specimen on PDMS was mounted in the load frame of test setup (Fig. 2.1). The tensile s train loading/unloading was commanded stepwise by 0.05 mm increment. Pristine PANI-based thin film specimen was first tested by subjecting the specimen to one cycle of tensile strain loading to ~1.28% and

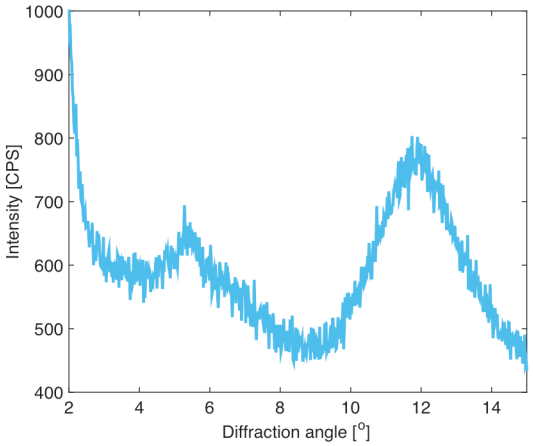

Figure 3.1 X-ray diffraction testing result confirms the crystalline structures of P3HT conjugated polymers in #2 P3HT-based thin film. Two peaks at ~5° and ~12° indicate diffracted X-ray counted per second (CPS) by crystalline P3HT formed with a distance 1.61 nm and 0.38 nm.

unloading to 0%. At each tensile strain level, light transmittance spectrum was acquired in light wavelength range from 300 nm to 1,100 nm. Next, pH 1 was simulated on the PANI-based thin film specimen using pH 1 buffer. This pH 1 buffer-treated specimen's light transmittance spectrums were obtained at various tensile strain levels over one cycle of tensile strain loading and unloading. Using the same specimen, this mechano-optical characterization testing was repeated but with other six pH buffers, such as pH 3, 5, 7, 9, 11, and 13, sequentially. PANI-based thin film specimen was loaded up to ~1.28% and unloaded to ~0%. Light transmittance of the P3HT-based thin film specimen was interrogated using UV-Vis spectrophotometer at each tensile strain level. Total 21 light absorbance spectrums were acquired during one cycle of tensile loading and unloading.

3. RESULTS AND DISCUSSIONS

3.1. Crystalline structures of P3HT

Long chain P3HT conjugated polymers tend to form crystalline structures in solid thin films. P3HT molecules are arrayed with a distance *a* on a plane, which is named as lamella, and the lamella is stacked up with a distance *b*. XRD technique was used for quantifying the crystallinity of the P3HT molecules by counting the number of crystalline structures formed with a distance *a* in (h00) direction and a distance *b* in (0k0) direction. Because optoelectronic properties of P3HT molecules are affected by the extent of alignment (*i.e.*, crystallinity) of the long chain polymers, it is crucial for P3HT molecules to form crystalline structures. Fig. 3.1 shows the XRD results obtained from the #2 P3HT-based thin film specimen. It is observed that there are two significant peaks at ~5° and ~12°, which indicate the diffracted X-ray by *a*- and *b*-distanced crystalline structure,

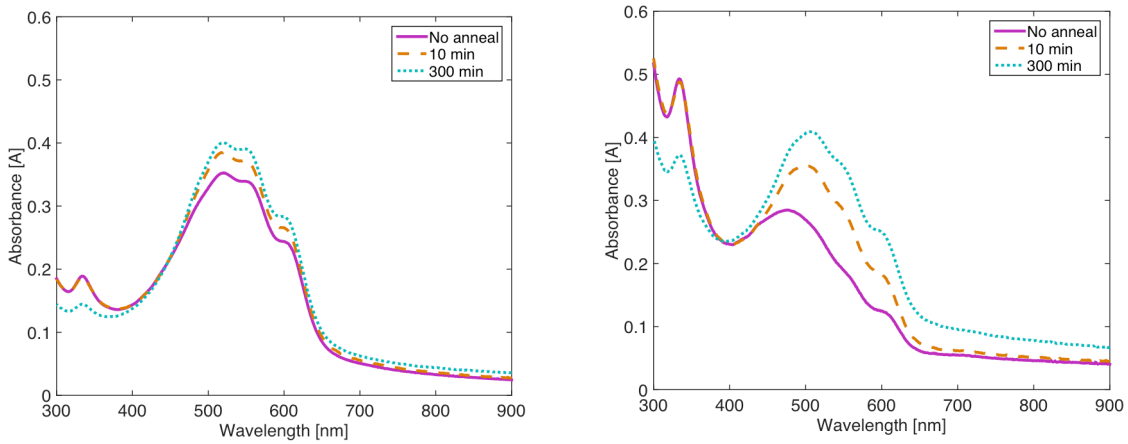

Figure 3.2 Light absorbance spectrums are shown from two representative as-produced and annealed P3HT-based thin films fabricated using (a) #1 (1:0.5 *w/v%*) and (b) #3 (1:1.5 *w/v%*) P3HT/PCBM-DCB solutions.

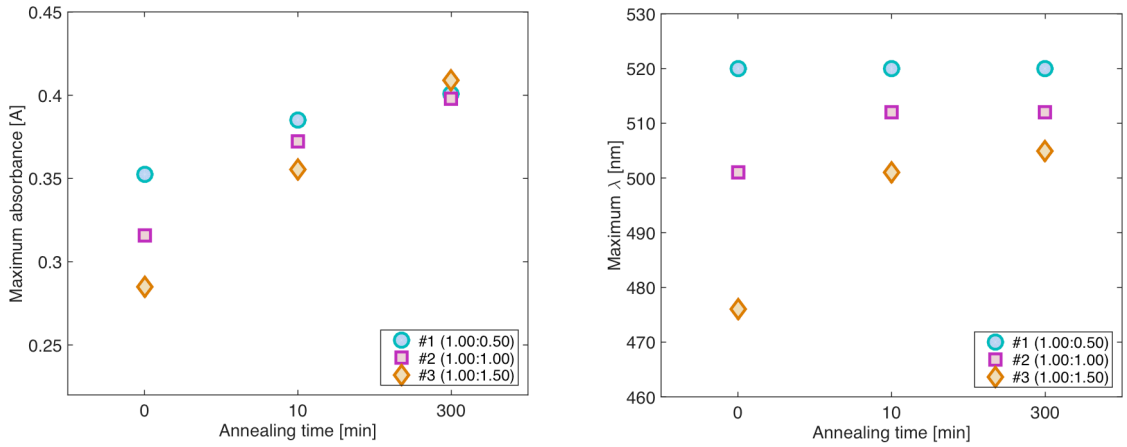

Figure 3.3 Major peak characteristics due to intrachain π-π^* electron transition of P3HT is shown for #1, #2, and #3 P3HT-based thin films for various annealing time: (a) absorbance and (b) wavelength.

respectively. It should be noted that P3HTs are distanced by a=1.61 nm on a lamella and each lamella is stacked with a distance of b=0.38 nm.

3.2. Thermo-optical properties of P3HT

There are several factors that affect the formation of crystalline structures, effective conjugation length, and optical properties of the conjugated polymers. Among the factors, it was shown that annealing process was very effective with improving crystallinity of P3HT molecules [10-12]. To investigate annealing time and temperature effect on the crystallinity of P3HT based on the optical light absorbance, three different P3HT-based thin films prepared using #1, #2, and #3 PPD solutions were tested.

First, the as-produced and annealed specimens were interrogated with UV-Vis spectrophotometer. Annealing temperature was 150°C, and annealing time varied to be 10 min and 300 min. Fig. 3.2 shows UV-Vis light absorbance spectrums of two representative #1 and #3 P3HT-based thin films. It can be seen that there are two major peaks at ~330 nm and ~510 nm and two minor peaks at ~550 nm and ~600 nm in the light absorbance spectrums. In particular, it should noted that the major peak at ~510 nm and two minor peaks at ~550 nm and ~600 nm are attributed to photons absorbed by P3HT molecules. The major peak at 510 nm indicates intrachain π-π^* electron transition along the P3HT molecules' backbone [10]. Minor peaks are attributed to the interchain electron transitions between P3HT molecules. The major peak at ~330 nm is due to light absorption by PCBM. In the UV-Vis light absorbance plots of Fig. 3.2, it can be observed that overall light absorbance due to P3HTs increases as the P3HT-based thin films are annealed and annealing time increases. This increasing trend of light absorbance shows that annealing improved P3HT molecules' alignment and light absorptivity. It is because light absorptivity of P3HTs is influenced by the linearity of P3HT while well-packed P3HTs tend to be more aligned

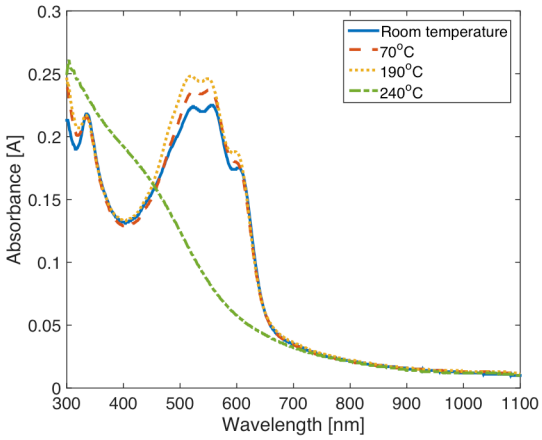

Figure 3.4 #2 P3HT-based thin film was annealed at various temperatures for 10 min each.

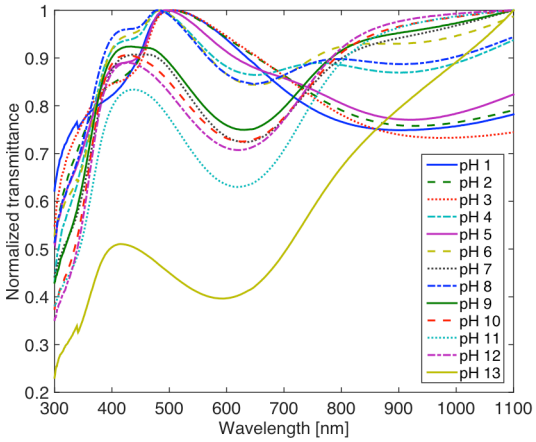

Figure 3.5 Light transmittance spectrums of PANI/PSS thin film are presented after treating with thirteen pH buffers.

[10]. In addition, when comparing two sets of light absorbance spectrums in Fig. 3.2a and b, the peak is more broadened as PCBM concentration increases. It is because PCBM hinders P3HT molecules' ordered packing to be less effective in light absorption.

Furthermore, intrachain electron transition of P3HTs was analyzed by plotting light absorbance and wavelength at the major peak, which are shown in Fig. 3.3a and b. As already observed in Fig. 3.2, light absorbance increases as annealing time increases. As PCBM concentration increases, annealing improved more effectively with light absorbance of P3HT. Meanwhile, it can be seen that annealing shifted the major peaks in Fig. 3.3b. For the # 1 P3HT-based thin film, there is negligible shifting of peak. But, ~25 nm red shift was observed for the #3 P3HT-based thin film. It should be noted that peak wavelength is correlated to the effective conjugation length of P3HT, and more aligned P3HT shows longer peak wavelength. Here, we can conclude that annealing helped P3HT alignment and is more effective when there is higher PCBM concentration in P3HT-based thin film.

Second, #2 P3HT-based thin film was annealed at various temperatures to investigate the effect of temperature effect on light absorbance. Fig. 3.4 shows four light absorbance spectrums, which were acquired after 10 min annealing at each annealing temperature. It can be seen that high temperature annealing at 240°C can deteriorate P3HT-based thin films and its light absorptivity. It is thought that P3HT and PCBM were melted at high temperature.

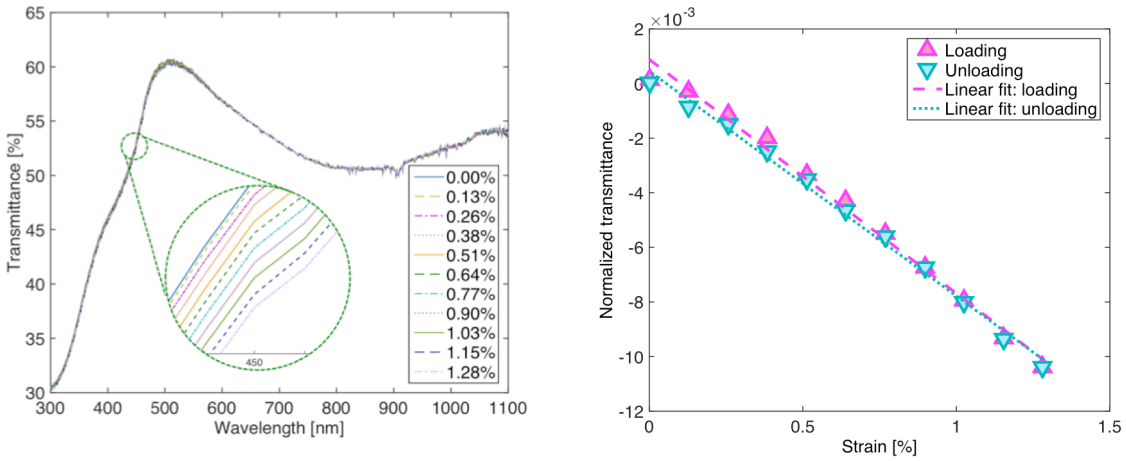

(a) (b)

Figure 3.6 (a) Light transmittance of PANI-based thin film after pH 1 buffer treatment is shown during strain loading. (b) Normalized transmittance at 450 nm is plotted with applied tensile strain.

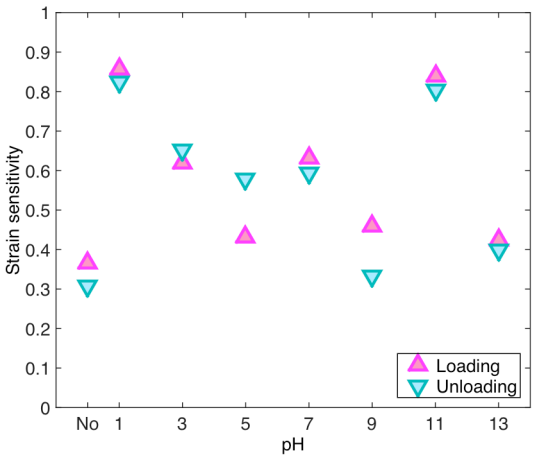

Figure 3.7. Strain sensitivities of the PANI-based thin films are plotted with various pH levels.

3.3. Chemo-optical properties of PANI

It was shown that PANI-based thin films exhibited colorimetric pH sensing capability [9, 13]. To better understand the chemo-optical properties of PANI-based thin films, light transmittance of the PANI-based thin films was obtained after treating the PANI-based thin film with thirteen different pH buffers. Fig. 3.5 shows the chemo-optical test result where each light transmittance spectrum was normalized by the maximum light transmittance of each spectrum to clearly show the peak shift. Overall, it can be observed that peak of the PANI-based thin film's light transmittance was abruptly shifted when the film began being treated with pH 7 buffer. In acid environment, PANI-based thin film showed more greenish color due to peak at ~500 nm. On the other hand, in alkaline range, the peak at ~420 nm contributed to blue/purple color change of PANI-based thin film. It should be noted that the pristine PANI-based thin film showed blue/purple color. Valley at ~620 nm for the light transmittance spectrums, which corresponds to light absorption, of alkaline pH buffer-treated PANI-based thin films results from π-π^* electron transition [10, 14]. On the other hand, a broad valley above 800 nm in the light transmittance spectrums in strong acid (*i.e.*, pH 1-5) is due to protonated electron transition [10, 14].

3.4. Mechano-optical properties of PANI

PANI-based thin film specimens fabricated on PDMS substrates were subjected to various tensile strains during one cycle of loading and unloading. As-prepared specimen and pH buffer-treated specimens were tested. Fig. 3.6a shows light transmittance spectrums during tensile strain loading of pH 1 buffer-treated PANI-based thin films. It can be seen that overall transmittance decreases as applied tensile strain increases. Transmittance at 450 nm was chosen and normalized by the transmittance at 0% strain to be plotted with applied tensile strain (Fig. 3.6b). Two least squares regression lines were overlaid with the normalized light transmittance during loading and unloading. The absolute value of the slope of regression line is considered as strain sensitivity and plotted with pH level of buffer used for treating PANI-based thin film in Fig. 3.7. It is shown that light transmittance of the PANI-based thin film varies with applied tensile strain, and mechano-optical properties of the PANI-based thin films are influenced by the pH level.

4. CONCLUSIONS

In this study, multiphysics-optical properties of P3HT- and PANI-based thin films were studied. These two thin films were used for fabricating multi-modal thin film sensors for selectively monitoring cracks and corrosion. The multi-modal sensor used intrinsic optical properties of the two P3HT-based and PANI-based thin films at various conditions (*i.e.*, tensile strain and pH). To understand its thermo-, chemo-, and mechano-optical properties of the two sensing thin films, two analytical spectroscopic techniques (*i.e.*, XRD and UV-Vis spectrophotometer) were employed.

First, P3HT-based thin films were interrogated with XRD to quantify crystalline structures of P3HTs. P3HT molecules were shown to be organized in three-dimensional space by forming lamellae structures with featured distances, such as 1.61 nm and 0.38 nm. Second, annealing effect was investigated on the crystalline structures

and molecular alignment of P3HTs using UV-Vis spectrophotometer. It was shown that annealing improved light absorptivity of P3HT-based thin films due to better packing and alignment of P3HT molecules within the thin films. This conclusion was supported by the red-shift of light absorbance peak and eminent peaks after annealing. In addition, inclusion of PCBM was shown to have adverse effect in crystalline structure formation of P3HTs. Third, PANI-based thin films' chemo-optical and mechano-optical properties were studied. Depending on the extent of protonation of emeraldine salt PANI, light transmittance of the PANI-based thin films varied while exhibiting peak shift and color change. It was also shown that the light transmittance of the PANI-based thin films decreased as the thin film is stretched during tensile strain loading cycle. When the applied tensile strain is removed, the light transmittance elastically returned to original state. The mechano-optical properties of the PANI-based thin films were affected by pH level.

ACKNOWLEDGEMENT

Authors would like to express their gratitude to National Science Foundation (Grant number: CMMI 1031754; PI: Prof. Kenneth J. Loh, University of California, Davis) for supporting this research. Also, we thank New Mexico Tech to provide partial support for the research.

REFERENCES

1. Lynch, J.P., and Loh, K.J. (2006). A Summary Review of Wireless Sensors and Sensor Networks for Structural Health Monitoring. *The Shock and Vibration Digest*. **38:2**, 91-128.
2. Sohn, H. (2007). Effects of Environmental and Operational Variability on Structural Health Monitoring. *Philosophical Transactions of the Royal Society A: Mathematical, Physical and Engineering Sciences*. **365:1851**, 539-560.
3. Zagrai, A., Doyle, D., Gigineishvili, V., Brown, J., Gardenier, H., and Arritt, B. (2010). Piezoelectric Wafer Active Sensor Structural Health Monitoring of Space Structures. *Journal of Intelligent Material Systems and Structures*. **21:9**, 921-940.
4. Kahandawa, G.C., Epaarachchi, J., Wang, H., and Lau, K.T. (2012). Use of FBG Sensors for SHM in Aerospace Structures. *Photonic Sensors*. **2:3**, 203-214.
5. Venancio, P.G., Cottis, R.A., Narayanaswamy, R., and Fernandes, J.C.S. (2013). Optical Sensors for Corrosion Detection in Airframes. *Sensors and Actuators B: Chemical*. **182**, 774-781.
6. Bahn, C.B., Bakhtiari, S., Park, J., and Majumdar, S. (2013). Manufacturing of Representative Axial Stress Corrosion Cracks in Tube Specimens for Eddy Current Testing. *Nuclear Engineering and Design*. **256**, 38-44.
7. Elfergani, H.A., Pullin, R., and Holford, K.M. (2013). Damage Assessment of Corrosion in Prestressed Concrete by Acoustic Emission. *Construction and Building Materials*. **40:0**, 925-933.
8. He, Y., Tian, G., Zhang, H., Alamin, M., Simm, A., and Jackson, P. (2012). Steel Corrosion Characterization Using Pulsed Eddy Current Systems. *IEEE Sensors Journal*. **12:6**, 2113-2120.
9. Ryu, D., and Loh, K.J. (2014). Multi-Modal Sensing Using Photoactive Thin Films. *Smart Materials and Structures*. **23:8**, 085011.
10. Skotheim, T.A., Elsenbaumer, R.L., and Reynolds, J.R. (1998). Handbook of Conducting Polymers, ed. Skothim, T.A., Elsenbaumer, R.L., and Reynolds, J.R. Marcel Dekke, Inc.: New York, NY.
11. Li, G., Shrotriya, V., Yao, Y., and Yang, Y. (2005). Investigation of Annealing Effects and Film Thickness Dependence of Polymer Solar Cells Based on Poly(3-Hexylthiophene). *Journal of Applied Physics*. **98:4**, 043704.
12. Motaung, D.E., Malgas, G.F., Arendse, C.J., Mavundla, S.E., Oliphant, C.J., and Knoesen, D. (2009). Thermal-Induced Changes on the Properties of Spin-Coated P3HT:C60 Thin Films for Solar Cell Applications. *Solar Energy Materials and Solar Cells*. **93:9**, 1674-1680.
13. Grummt, U.-W., Pron, A., Zagorska, M., and Lefrant, S. (1997). Polyaniline Based Optical pH Sensor. *Analytica Chimica Acta*. **357:3**, 253-259.
14. Tsai, Y.-T., Wen, T.-C., and Gopalan, A. (2003). Tuning the Optical Sensing of pH by Poly(Diphenylamine). *Sensors and Actuators B: Chemical*. **96:3**, 646-657.